Dark-binding process relevant to preventing photosensitized oxidation: Conformation dependent light and dark mechanisms by a dual-functioning diketone

Sarah J. Belh[†,‡], Niluksha Walalawela[†,‡], Stas Lekhtman[†], and Alexander Greer[†,‡,*]

[†]Department of Chemistry, Brooklyn College, 2900 Bedford Avenue, Brooklyn, New York 11210, United States

[‡]Ph.D. Program in Chemistry, The Graduate Center of the City University of New York, 365 Fifth Avenue, New York, New York 10016, United States

E-mail: agreer@brooklyn.cuny.edu

Abstract

Few photosensitizers function in both light and dark processes, as they usually have no function when the lights are turned off. We hypothesized that light and dark mechanisms in an α-diketone will be decoupled by dihedral rotation in a conformational-dependent binding process. Successful decoupling of these two functions is now shown. Namely, *anti* and *syn*-skewed conformations of 4,4'-dimethylbenzil promote photosensitized alkoxy radical production, whereas the *syn* conformation promotes a binding shut-off reaction with trimethyl phosphite. Less rotation of the diketone is better suited to the photosensitizing function since phosphite binding arises through the *syn* conformer of lower stability. The dual-function seen here with the α-diketone is generally not available to sensitizers of limited conformational flexibility, such as porphyrins, phthalocyanines, and fullerenes.

Introduction

Dual-functioning compounds, such as those which perform as both imaging agents as well as photosensitizers, are an increasing class of compounds.[1-3] Dual functioning has been approached from many different angles.[4,5] In one case, singlet oxygen ($^1O_2$) was used to photodegrade micelles for the delivery of the doxorubicin for combined $^1O_2$ and drug activity (Figure 1).[6] In this case,[6] the photochemical and dark functions relate to a drug release process.

However, there is a way to go before photosensitizers can also serve simultaneously as chemotherapeutic drugs. Here, we describe an α-diketone sensitization that responds as a conformational switch to binding which may bring the goal a step closer. Conformationally-dependent binding of drugs that shut off the photosensitization pathway are generally not exploited in photodynamic therapy (PDT). The reason is that conformational twisting is almost never available to sensitizers as they are often cyclic structures. In the case of porphyrins and phthalocyanines, a flat shape is largely retained upon excitation. Sensitizers that can adopt flat *and also* twisted conformations are in need of greater study in the context of dual function. Tools from the perspective of conformational binding can then influence the outcome of the photooxidation. The two functions (i.e., light and dark) can that come together to influence each other in competitive reactions.

The potential for such dual-functioning compounds are α-diketones (diones) that are now explored for chemical binding vs photosensitization processes. We hypothesized that a dione will act as a sensitizer as the *anti* isomer and undergo chemical binding as the *syn* isomer in a "give and take" to the sensitization process (Figure 2). That compounds may be decoupled from sensitization through drug binding would be of fundamental interest.

Dione compounds have been shown to act well as binding agents, including in enzyme active sites.[7] For example, benzils bind to tubulin proteins in a similar manner as stilbenes, such as combretastatin A-4.[8] Furthermore, diones have been shown to be important in chelation reactions with phosphites,[9,10] and have been used in the synthesis of phosphoranes.[11] Diones such as 4,4′-dimethylbenzil (**1**) and mono-carbonyl compounds have been used as photosensitizers in photooxidation reactions,[12-15] but not in the terms of dione conformational binding and photosensitization as we describe here. Indeed, the dual functionality of diones for photosensitization and subsequent binding has not been previously explored.

We report on a conformational switch between dione-sensitized peroxide decomposition and dione binding to phosphite. Tuning the dione conformation is desired not only to thermally chelate, but control peroxide sensitization to alkoxy radicals, in which Light Path A and Dark Path B are competitive (Figure 3). The dione sensitization is permanently shut off by a conformational switch in phosphite binding. We now demonstrate that *anti* and *syn-skewed* conformations of **1** promote sensitization, whereas the *syn* conformation promotes phosphite binding. The following presentation only considers 4,4′-dimethylbenzil **1** and glyoxal (oxalaldehyde) **2**; the former in experimental and theoretical work, the latter only in theoretical work. Dicumyl peroxide [(peroxybis(propane-2,2-diyl))dibenzene] **3** was the peroxide used in these experiments. The mechanism in Figure 3 is consistent with the data collected, as we will see next.

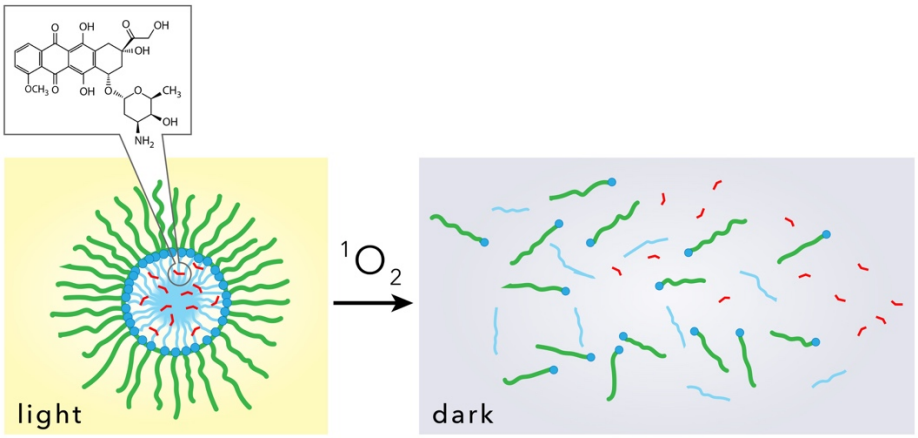

Figure 1. Micelle degradation by photogenerated singlet oxygen for the release of doxorubicin.

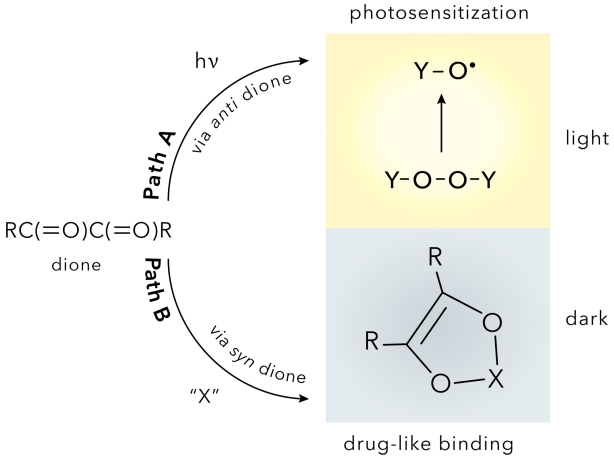

Figure 2. Conformational switch of dione for photosensitized oxidation activity and binding activity. The dione acts as a photosensitizer (Path A) and binds to a phosphite shutting off the sensitization (Path B). It will be shown how paths A and B are competitive. Dione concentrations and the proticity of the surrounding environment is tested. Here, "X" represents a chelating agent such as protein binding site or a phosphite molecule as is examined in the current work.

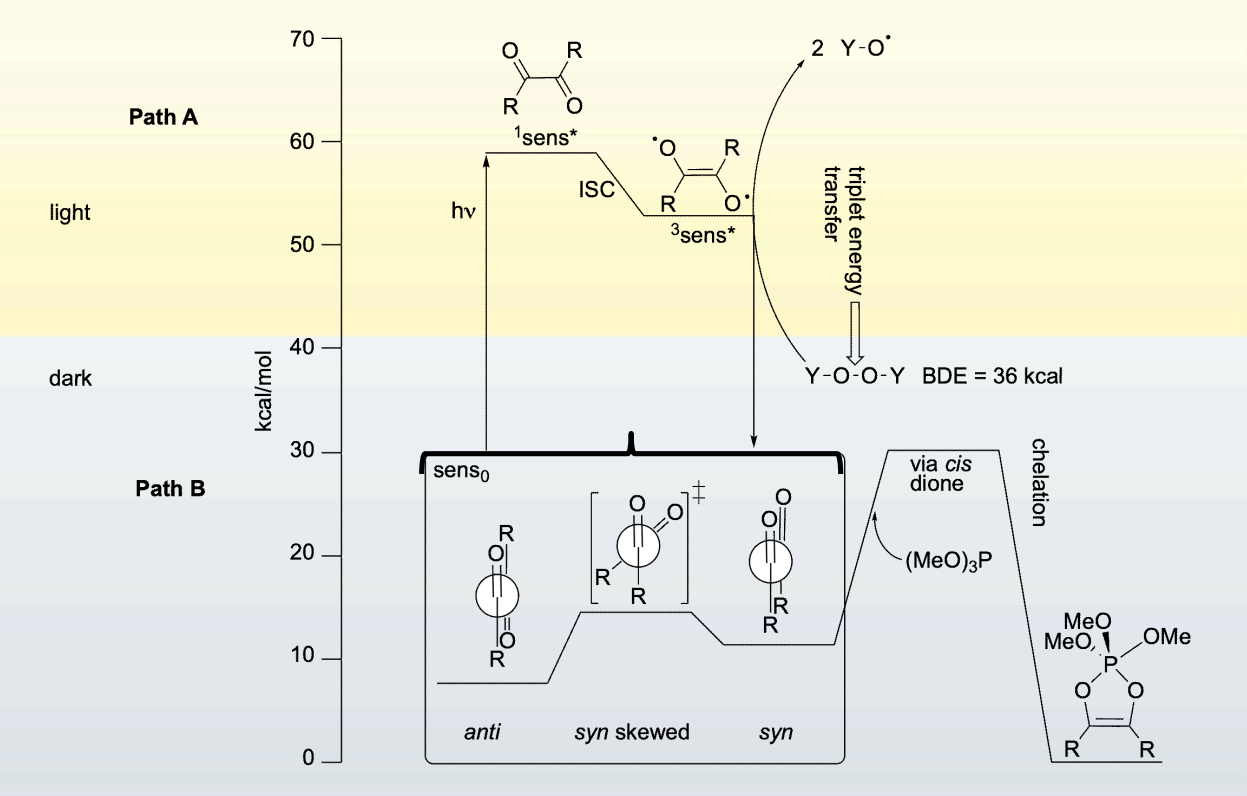

Figure 3. Proposed mechanism that blends the dark (thermal) and light (Jablonski-like) processes. The 1,2-dione sensitizer is competitive in photodecomposition of dicumyl peroxide **3** (Path A) and binding of *syn* dione with $(MeO)_3P$ (Path B). The energetics for the Jablonski diagram (upper portion) were estimated from literature data. Aprotic and protic media influence the reaction of the alkoxy radical. The alkoxy radical also competes with the 1,2-dione for the $(MeO)_3P$ trapping agent. Phosphorane **4** (R = *p*$CH_3C_6H_4$); phosphorane **5** (R = H). "Y" is the $C_6H_5C(Me_2)$ group on dicumyl peroxide **3**.

Results

The results are presented in the following four subsections: (1) the computed binding process between dione **2** and $(MeO)_3P$; (2) analysis of the kinetics of the binding; (3) the sorting out the contributions from light and dark reactions; and (4) the product distribution upon photosensitized homolysis dicumyl peroxide **3**.

Dihedral Rotation Dependence of Bidentate Binding. Some details of the dione rotation and phosphite binding can be obtained from DFT calculations. Dione **2** was used as a model system to mimic the 1,2-dione portion of 4,4′-dimethylbenzil **1** due to lower computational cost of the former. Dione **2** serves as a model for the DFT calculations, but is not a good sensitizer. Figure 4 shows the B3LYP/D95(d,p) energies for the rotation of dione **2** around the dihedral angle (θ for O=C–C=O), which was constrained to 10° increments. The *anti* rotamer is the global minimum, and the *syn* rotamer is 5.6 kcal/mol less stable. The *syn* rotamer is reached by a *syn*-skewed transition structure with a barrier height of 7.5 kcal/mol. For the larger dione (dimethylbenzil, **1**), a pure *syn* geometry of **1** cannot be transposed on its core, and therefore a *syn*-skewed minimum is favored due to a buttressing of the nearby aryl groups, which destabilize the *syn* geometry. It appears that the *ortho*-aryl hydrogens disable dione **1** from adopting a pure *syn* geometry. Nonetheless, **2** served as a good model for the 1,2-dione segment of **1**. Relatedly, Allonas et al.[16] describe the importance of diones in a photochemical reaction. In their reaction, diones restricted to the *syn* conformation bore lower E_T values by a couple of kcal/mol compared to diones equilibrating both *syn* and *anti* conformations. In our case, a computed rotational profile is featured for a *syn* and *anti* dione, where both are stable, however the less stable *syn* dione reacts with $(MeO)_3P$ through an equilibrium process.

Next, we computed the cyclization path of dione **2** with $(MeO)_3P$. This binding reaction arises from the *syn* dione. The transition structure for the cyclization is shown in Figure 4, where the resultant dihedral angle (θ is O=C–C=O) is approximately planar for **TS2/3** is 0.9°. The phosphorane **5** possesses a trigonal bipyramidal geometry, where the apical P–O bond distance (2.37 Å) is longer than the equatorial P–O bond distance (2.18 Å). The activation energy for the association of dione **2** with $(MeO)_3P$ is predicted to be $\Delta E^{\ddagger}$ = 15.3 kcal/mol. Only a transition structure for a concerted process from the *syn* dione was found. Transition structures for a step-wise addition could not be located. We also did not find an energy minimum for a monodentate binding between dione **2** and $(MeO)_3P$. Formation of peroxide **3** is exothermic by 9.1 kcal/mol compared to the reagents **1** and **2**. The decomposition of phosphorane is a high-barrier process so that it irreversibly ‘‘masks’’ dione **2**, where the energy barrier for the release of phosphite from the phosphorane is 30.0 kcal/mol. An assessment of molecular orbitals (MOs) was as also informative to understanding the free form of the dione and the phosphite binding process.

DFT computations show that the phosphite HOMO is of σ character and can donate to the syn dione **2** LUMO in a symmetry allowed process (Figure 5). The HOMO of dione **2** contains π* orbitals on the C=O bonds, and π bonds are formed in the P–O groups of the phosphorane **5**. The chelation of $(MeO)_3P$ to the dione likely alters the electronic transition of the dicarbonyl group. The experimental results show that α-diketones bear strong *n*,π* character,[16] which is reduced in the phosphorane **5**. Next, we present experimental evidence for a cyclization of dione **1** with $(MeO)_3P$ to reach phosphorane **4**.

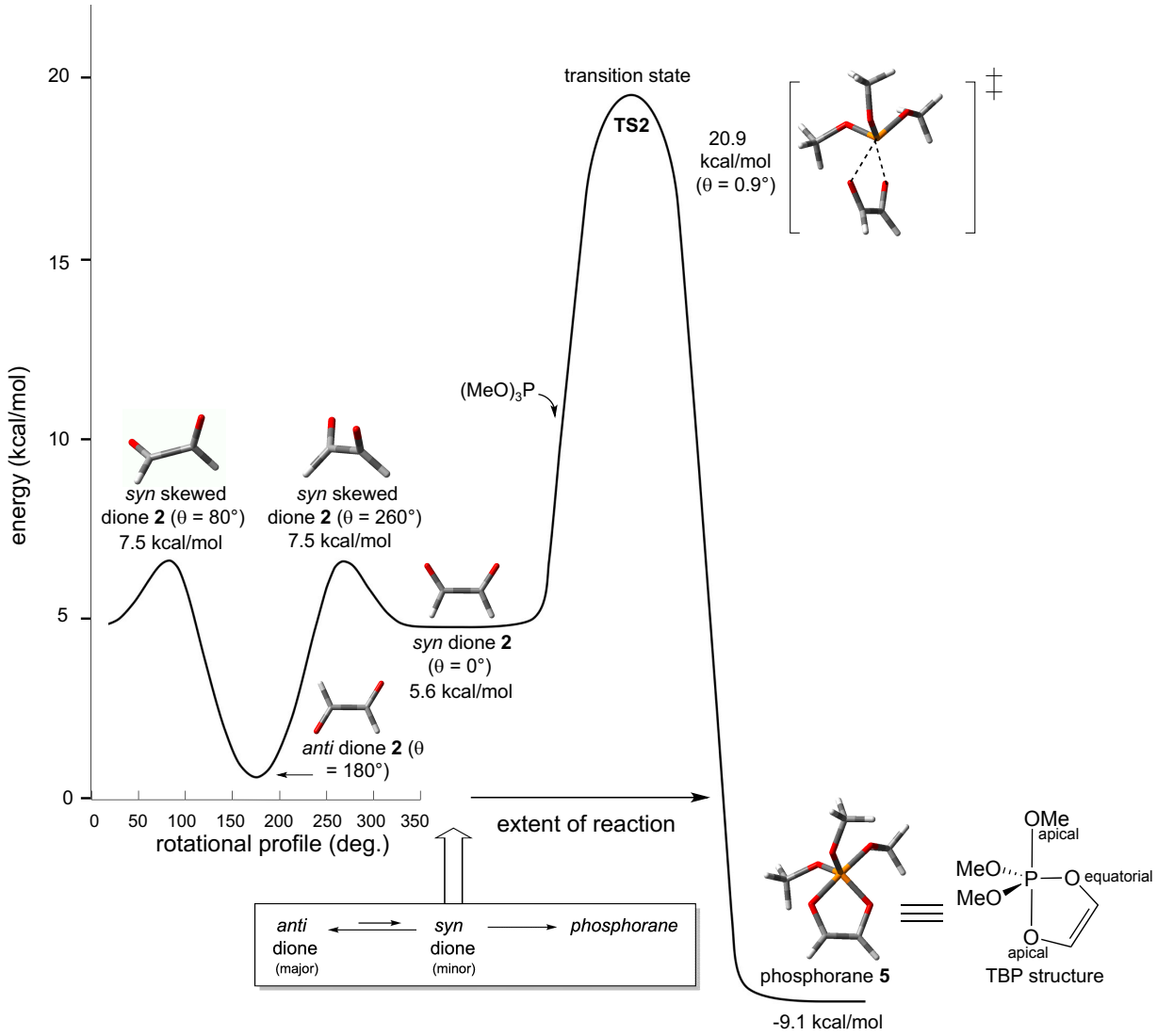

Figure 4. DFT computed energy plot for the 360° rotation of the 1,2-dione group in **2**, and potential energy surface for the reaction of **2** with $(MeO)_3P$. θ is the dihedral angle for O=C–C=O of the dione. Oxygen atoms are red, carbon atoms are gray, and hydrogen atoms are white.

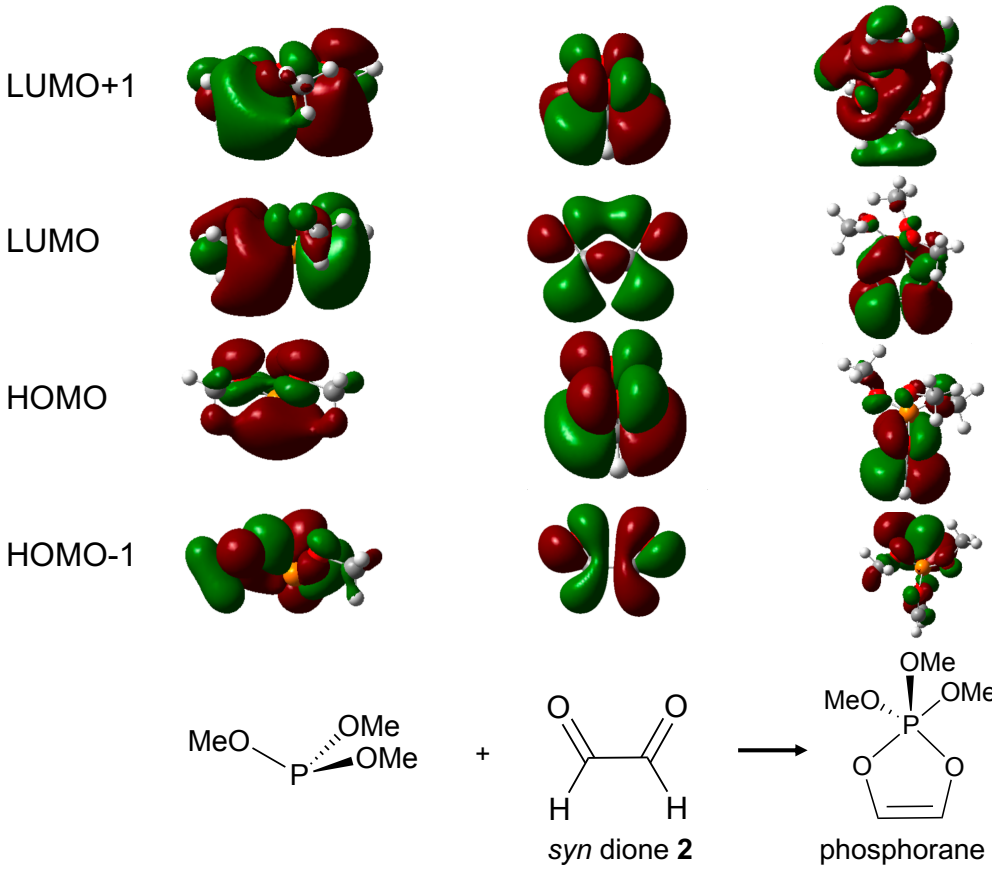

Figure 5. DFT computed HOMO and LUMO of *syn*-dione **2**, $(MeO)_3P$, and phosphorane **5**. Oxygen atoms are red, carbon atoms are gray, and hydrogen atoms are white.

Kinetics of Dione Binding to Phosphite. We sought experimental evidence for the formation of phosphorane **4** since dione **1** is a sensitizer. Figure 6 shows the reaction of dione **1** with $(MeO)_3P$ over time. Figure S8 (Supporting Information) show a near-linear pseudo-first order fits for their disappearance. Due to the sparing stability of phosphorane **4**, kinetics for its disappearance do not fit first order kinetics. Phosphorane **4** is an intermediate and exists for ~10

minutes as a mixture in the reaction. Notice the absorptivity of dione **1** decreases when chelated to $(MeO)_3P$ upon formation of the phosphorane **4**. A weak phosphorane absorption is attributed to a π,π^* transition that appears at a shorter wavelength (λ_{max} = 235 nm) in comparison to dione **1** (λ_{max} = 270 nm), although the phosphorane still bears an n,π^* transition. The transient phosphorane **4** was detected by ^1H NMR (doublet "b" is located at 3.66 and 3.69 ppm) (Figure S2), where its location is similar to $POCH_3$ peaks in phosphorane compounds previously reported.[11] The ^{31}P NMR data also show evidence for the phosphorane **4** (-49.6 ppm) (Figure S4) in which the phosphorus atom is covalently bound to five oxygen atoms. Similar negative chemical shifts have been observed for other phosphoranes.[12]

The appearance of trimethylphosphate $[(MeO)_3P{=}O]$ is a consequence of the phosphorane **4** decomposition via aryl migration, a side reaction leading to ketene. Based on the literature of ketenes,[11] phosphorane **4** cleavage is expected to lead to $(p\text{-}MeC_6H_4)_2C{=}C{=}O$ and $(MeO)_3P{=}O$, and by-products, although we did not analyze these downstream reactions. Next, we sought to examine the competitive binding of dione **1** with $(MeO)_3P$ (Dark Path B) and the photooxidation activity in cumyloxy radicals generated in dicumyl peroxide **3** photodecomposition (Light Path A).

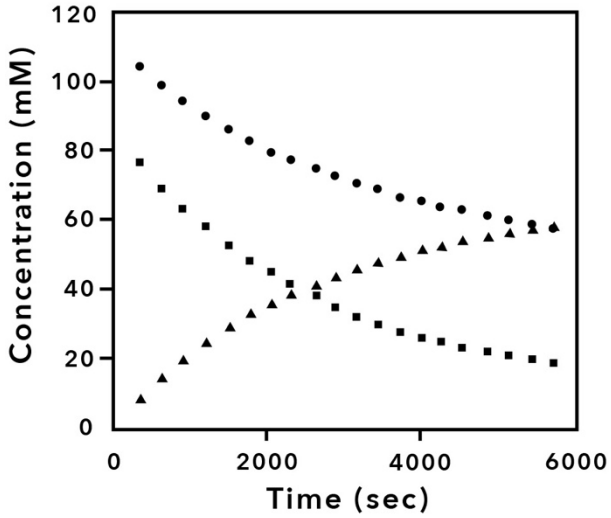

Figure 6. Plot of the disappearance of 4,4′-dimethylbenzil **1** (●) and $(MeO)_3P$ (■), and appearance of phosphorane **4** (▲) over time in CH_3CN.

Separating the Light and Dark Paths. In addition to phosphite chelation to dione (Path B), we show that phosphite can be used to indirectly monitor the photodecomposition of dicumyl peroxide, by trapping the resultant cumyloxy radicals (Light Path A) (Table 1). The use of phosphite as alkoxy radical traps is reported in the literature.[17,18] Table 1 shows the dione **1** sensitized dicumyl peroxide **3** decomposition as a function of the sensitizer to peroxide ratios. The ratios correspond to concentrations of 100 mM **1** and 0.5 to 100 mM **3**. Data are shown for $(MeO)_3P{=}O$ formed from Light Path A, Dark Path B, and combined Paths A + B. Samples were irradiated in N_2-sparged solutions with $300 < \lambda < 700$ nm light from 400-W metal halide lamps with a fluence of 21.8 mW/cm^2. Table 1 (column 5) are the data for tracking the loss of dicumyl peroxide **3** in the photoreaction. The sensitizer/peroxide ratio of 1:1 showed an 9%

increase in peroxide homolysis compared to the 1:10 ratio (entries 1 and 2). Thus, the photosensitized decomposition of **3** was about 3 times more rapid in the 1:1 ratio sensitizer/peroxide compared to the 1:10 ratio. As we see, the sensitized **3** decomposition was shown to require a high sensitizer to peroxide ratio. Ratios of 1:40 or lower (entries 3-5) show no detectable sensitized decomposition of dicumyl peroxide **3**. The amount of phosphate formed un the light (column 5) and dark (column 6) reactions can be readily determined. In the dark, the reaction of dione **1** and $(MeO)_3P$ led to phosphorane **4** and by-products based on UV-VIS and NMR data. After 41 min, the reaction mixture contained dione **1** and phosphorane **4** in a ratio of ~1:1 (Figure S7, Supporting Information). Entry 7 is a control experiment showing that no detectable amount of phosphate is formed over a 1 h period in the dark and in the absence of dicumyl peroxide and dione **1**.

Path B clearly is significant since Path A values are lower by comparison. In the absence of sensitizer, direct irradiation ($300 < \lambda < 700$ nm) leads to no detectable photodecomposition of dicumyl peroxide **3** (entry 6). Indeed, the poor excitation wavelength overlap of the dicumyl peroxide **3** with the light source provides an explanation for dicumyl peroxide's stability without sensitizer. While dicumyl peroxide **3** is photochemically unstable with UVC light (data not shown), our light source is mainly UVA and visible light with some UVB, and thus we demonstrate that dione sensitizer **1** leads to the photolability of dicumyl peroxide **3**. The extent of peroxide decomposition due to direct irradiation ($280 < \lambda < 700$ nm) is negligible for dicumyl peroxide **3** (~0%) under our conditions. Thus, it follows that the fragility of peroxide O–O bonds needs to be negligible for quantitation of any sensitized contribution to the decomposition. Next, we carried out DFT studies to probe the dicumyl peroxide O–O bond dissociation further.

Since the dicumyl peroxide **3** is not excited, we conducted ground-state DFT calculations rather than TD-DFT calculations to predict the energetics for O–O bond dissociation on the singlet and triplet potential energy surfaces (PESs). The O–O bond was elongated and optimized at each distance with the resulting potential energy curves shown in Figure 7. It is readily seen that on the singlet surface, O–O bond separation is endothermic with a barrier to O–O bond homolysis of ~60 kcal/mol. In contrast on the triplet surface, the O–O bond separation is exothermic and that the forming cumyloxy radical pair are strongly repulsive. The singlet surface in Figure 7A shows the separated cumyloxy radicals are found oriented in an *anti*-conformation. On the singlet surface, the homolysis would is high in energy to unveil alkoxy radicals. On the other hand, the triplet surface in Figure 7B shows the separated cumyloxy radicals remains in a *cis* skewed conformation even up to a separation distance of 3.5 Å. Based on these DFT results (Figure 7), and keeping in mind the O–O bond dissociation energy (BDE) of dicumyl peroxide **3** is 36 kcal/mol,[19,20] we surmise that the photosensitized O–O bond homolysis occurs on the triplet manifold via energy transfer to a repulsive orbital of the O–O bond. For releasing the cumyloxy radicals beyond their contact-pair as free species, a small amount of heat would then be required.

Table 1. Monitoring dicumyl peroxide photodecomposition as a function of sensitizer to peroxide ratio[a-c]

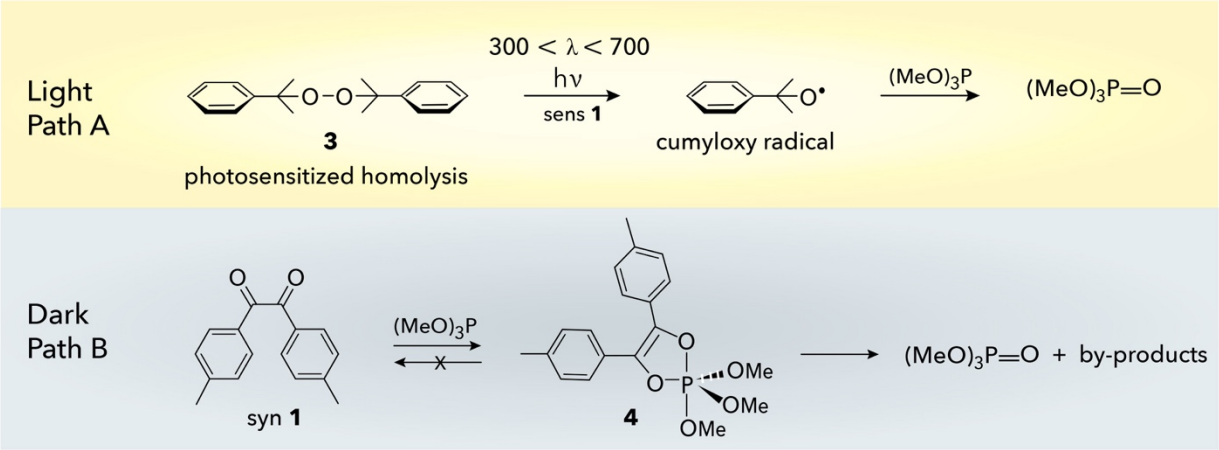

entry	dicumyl peroxide concentration (mM)	sensitizer **1** concentration (mM)	sensitizer **1** to peroxide ratio	loss of **3** from Light Path A[d] (mM)	phosphate formed from Dark Path B[d] (mM)	phosphate formed from Paths A + B[d] (mM)
1	100	100	1:1	14	37	51
2	100	10	1:10	5	15	20
3	100	2.5	1:40	0	12	12
4	100	1	1:100	0	14	14
5	100	0.5	1:200	0	15	15
6	100	0	0:1	0	0	0

7[e]	0	0	-	-	0	0

[a] Trimethylphosphite concentration was 100 mM. [b] Amount of phosphite and phosphate monitored by ^{1}H NMR (corresponding methyl peaks). [c] Amount of dicumyl peroxide **3** and products (cumyl alcohol and acetophenone) monitored according to HPLC. [d] Standard deviation is ±1%. [e] Sample was kept in the dark.

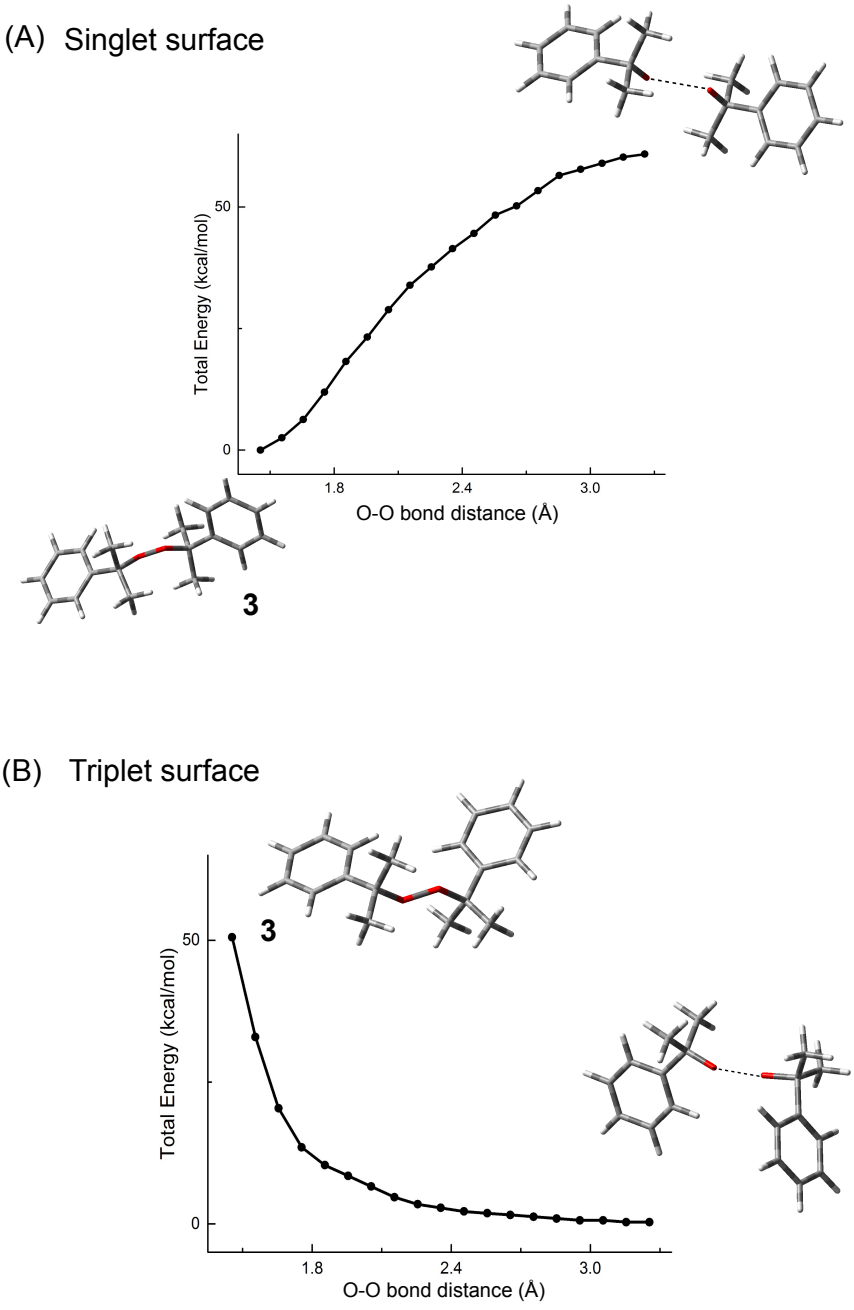

Figure 7. Unrestricted B3LYP/D95(d,p) calculations for the O–O bond dissociation of dicumyl peroxide **3** on the (A) singlet surface, and (B) triplet surface. The structures were optimized with the O–O bond was constrained by increases in 0.05 Å increments. Relative energies in kcal/mol.

Trapping of Photogenerated Cumyloxy Radical. As dicumyl peroxide **3** can be photosensitized to homolytically cleave, we turned to an evaluation of the effect of reaction medium on the product distribution to seek further evidence of the existence of cumyloxy radical. Table 2 show data which determine the effect of the surrounding media on the products formed in the 4,4′-dimethylbenzil **1** sensitized decomposition of dicumyl peroxide **3**. Here, acetophenone (**6**), 2-phenylpropan-2-ol (**7**), and α-methylstyrene (**8**) were detected as products. These products have higher triple state (E_T) energies than 4,4′-dimethylbenzil **1** and are not expected to serve as sensitizers, however their distribution depended on the presence or absence of an H-atom source.

In wet acetonitrile-d_3, irradiating with light from $300 < \lambda < 700$ nm, the products formed were acetophenone **6** (2%) and 2-phenylpropan-2-ol (**7**) (98%) (Table 2, entry 1). Somewhat similarly, a literature plasmon-excitation reaction in methanol showed dicumyl peroxide **3** decomposition to **6** (50%) and **7** (50%) (entry 2).[19] In contrast, in dry acetonitrile-d_3, products were favored in the opposite direction with the near exclusive formation of acetophenone **6** (99%), with 2-phenylpropan-2-ol **7** (<1%) and a trace amount of α-methylstyrene **8** (entry 3). Solution-free conditions on silica with unfiltered UV light ($280 < \lambda < 700$ nm) or with direct irradiation of **3** with 254 nm light in a container rotated by a stirring paddle to tumble the particles. The solution-free conditions led to a slightly reduced yield acetophenone **6** (67-70%), with 2-phenylpropan-2-ol **7** (4-5%), and α-methylstyrene **8** (1-2%) (entries 4 and 5). For the solution-free reactions on silica, the mass balance of the reaction was ~75% due to evolution of volatile species, such as CH_3• and CH_4. A literature plasmon-mediated reaction in acetonitrile also showed the main product to be **6** (98%) with a minor amount of **7** (2%) (entry 6).[19]

We attribute these results to cumyloxy radicals formed in the sensitized homolysis of dicumyl peroxide **3**, which abstracts H atoms from water (in wet acetonitrile) or silanol (SiOH) groups on the silica surface. The cumyloxy radical may also be reacting with water on adsorbed to the silica surface leading to increased percent yields of **7**. The heterogeneous experiment was carried out on silica with high relative amounts of SiOH groups for H-atom abstraction. Our results are consistent with literature reports of H-atom abstraction by cumyloxy radicals in polymer crosslinking and other reactions.[21,22]

Table 2. Effect of aprotic and protic media in products formed from the 4,4′-dimethylbenzil **1** sensitized photodecomposition of dicumyl peroxide **3**.

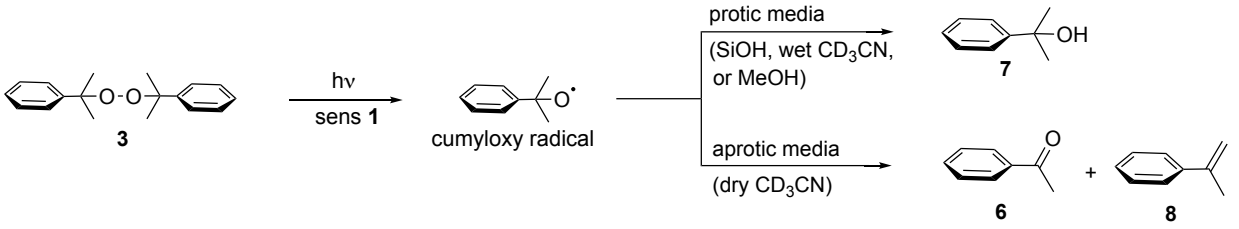

entry	reaction medium	condition	% yield of acetophenone **6** [g]	% yield of cumyl alcohol **7** [g]	% yield of α-methylstyrene **8** [g]	ref.
1	wet acetonitrile-d_3 solution[a,b,c]	dione **1** photosensitized	2	98	<0.01	this work
2	methanol solution	plasmon excitation	50	50	-	19

3	dry acetonitrile-d_3 solution[a,b]	dione **1** photosensitized	99	<1	<0.01	this work
4	gas/solid interface[a,d]	dione **1** photosensitized	70	4	1	17
5	gas/solid[a,e,f] interface	254 nm light	67	5	2	this work
6	acetonitrile solution	plasmon excitation	98	2	-	19

[a] An average of 3 runs with a standard deviation of ±3. [b] Irradiation at $300 < \lambda < 700$ nm. [c] Acetonitrile containing <1% H_2O. [d] Irradiation at $280 < \lambda < 700$ nm. [e] Solid phase is fumed silica. [f] Irradiation at 254 nm. [g] Sensitizedf homolysis of dicumyl peroxide **3** leads to cumyloxy radical, which adds to $(MeO)_3P$, and subsequently cleaves a methyl radical in reaching $(MeO)_3P{=}O$ based on the following proposed reaction: dione **1** + $Ph(Me_2)COO(Me_2)Ph$ **3** + hν → $2Ph(Me_2)CO\bullet$; $Ph(Me_2)COO(Me_2)Ph \leftarrow [2Ph(Me_2)CO\bullet] + (MeO)_3P \rightarrow (MeO)_3P{=}O$; $[2Ph(Me_2)CO\bullet] \rightarrow MeCOPh + Me\bullet$; $[2Ph(Me_2)CO\bullet]$ + H-atom source → ROH.

Discussion. We show that an equilibrium process of the less stable *syn* conformer of a dione binds to $(MeO)_3P$ irreversibly. The facility of this increases with the *syn* dione conformation. Since diones have been used as protein binding drugs,[7,8] there is a potential for their use in rotation tuning for binding from the *syn* form to sensitization from the *anti* form. That is, the function of the dione would be more photodestructive in the *anti* form, but more effective in protein binding

for example in the *syn* form. The competition for chemical selectivity (modulation response) emerges through an equilibrium process involving the less stable *syn* conformer. The transition state and formation of phosphorane arises from the *syn* dione according to the DFT calculations.

The photosensitized decomposition of dicumyl peroxide **3** requires relatively high concentrations of dione **1** and is proposed to take place on the triplet manifold. Cumyloxy radicals are formed and scavenge H-atoms from surface silanols, water adhered to silica, as well as methanol and water producing cumyl alcohol as the major product. In the peroxide-sensitized homolysis, H-atom abstraction of protic media by the cumyloxy radical is an important process that competes with methyl radical loss and formation of acetophenone as a major product in the dicumyl peroxide photodecomposition reaction. Dione **1** is not likely to photoreduce in the presence of water, but would be susceptible to photoreduction with H atom donors such as triethylamine or a phenol substituted with an electron donating substituent.[16] In terms of product formation, produced acetophenone (E_T = 74 kcal/mol) may also serve as a photosensitizer, although 4,4′-dimethylbenzil **1** has a fairly low-lying triple state (E_T = ~51 kcal/mol) is expected to be the main photosensitizer over the course of the peroxide **3** homolysis reaction. Also, for comparison O_2 degassed conditions were used otherwise a competing process would include dione sensitization to O_2 and formation of singlet oxygen. Our work is also part of a growing body of work[17,27-33] examining sensitization reactions by peroxide O–O bond homolysis, where the reaction is also relevant to the more commonly studied sensitization of $^3O_2$ to $^1O_2$.

Conclusion

We present a new concept for dark conformational dependence in connection with attenuating a photooxidation reaction. Namely, the ability of an α-diketone (4,4′-dimethylbenzil) to act as a photosensitizer for alkoxy radical production, and to bind to a trialkyl phosphite was studied in homogenous and heterogeneous systems. Upon binding to phosphite, the 4,4′-dimethylbenzil decreased in its alkoxy radical photoproduction, acting as a shut-off mechanism. This opens the avenue of α-diketones for prospective dual action in sensitization and in drug binding activity.

Diones such as **1** can serve as photosensitizers, but also have dark binding opportunities. The light and dark paths are competitive paths due to the rotational dependence about the two carbonyl groups, with the *syn* enhancing dark binding and the *anti* or *syn*-skewed increasing the light-dependent route. The system is a step toward the dual action goal, in which the design can be tailored to selected binding site to enhance cooperative dialog between phototherapy-to-drug binding. Such a collective mode of reaction is generally not available to sensitizer macrocycles with restricted conformational freedom.

Porphyrins have been studied and act well as $^1O_2$ sensitizers, but usually bind to membranes rather than within enzymatic pockets.[23] Porphyrin distortion away from planarity can lead to a shut off of their sensitizer activity,[24-26] however, porphyrins' large size mostly disallow competing processes, such as binding in a protein pocket. Here, we report on a dione that can bind a phosphite, an observation similar to the dione binding at metal active sites in enzymes (e.g., tropolones and hydroxy-tropolones), where the relative size of dione **1** and derivatives can facilitate binding. The effectiveness of the dione as a photosensitizer is suggested *but only* prior to binding, which suggests a potential advantage to dione-sensitized reactions in PDT applications.

Experimental

Computations. Calculations were carried out using Gaussian 09 (revision D.01)[36] with the B3LYP functional and the D95(d,p) basis set in gas phase. Molecules were visualized with GaussView 5.0.[37] The transition state structure **TS2** was verified as transition states by frequency calculations. Calculations were also carried out by scanning of bond rotations for dione **2** and the O–O bond dissociations of dicumyl peroxide **3** in the singlet and triplet surfaces by constraining compound geometries.

General. Reagents used include: 4,4′-dimethylbenzil **1**, dicumyl peroxide **3**, trimethylphosphite [$(MeO)_3P$], trimethylphosphate [$(MeO)_3P{=}O$], and triisopropylphosphate [(n-$C_3H_7O)_3P{=}O$] purchased from Sigma Aldrich and used as received. Potassium hydrogen phthalate from Fisher Scientific was used as received. Acetonitrile, acetonitrile-d_3, dichloromethane and methanol were purchased from VWR and used as received. The hydrophilic fumed silica particles used were 200-300 nm in diameter, with 200 ± 25 m^2/g surface area.

Photolysis Method. Figure S1 shows a schematic of irradiations that were conducted with samples placed in a 1-cm filter solution of 0.5 w/v% potassium hydrogen phthalate in water to collect light from $300 < \lambda < 700$ nm at the midpoint between two 400-W metal halide lamps, which delivered light ($280 < \lambda < 700$ nm). A handheld UV 254 nm light source was also used. Rises in temperature of ~2-3 °C were observed for the sample solution under irradiation after 1 h. We have previously measured the fluency rate at a mid-point in between the bulbs to be 21.8 ± 2.4 mW/cm^2.[34] The tail of the absorption of dione **1** (280-310 nm) overlaps with the output of the metal-halide light, but this overlap is poor and nearly nonexistent with dicumyl peroxide **3**, phosphorane **4**, $(MeO)_3P$, and $(MeO)_3P{=}O$. The compound, (n-$C_3H_7O)_3P{=}O$, was used as an

internal standard. Photolyses of dione **1** and dicumyl peroxide **3** were done in N_2-sparged solutions and heterogeneous samples, as described next.

Homogeneous Method. Typically, acetonitrile solutions were used containing dicumyl peroxide **1** (0.1 M) in the presence or absence of sensitizer 4,4′-dimethylbenzil **1** (0.01 M) and $(MeO)_3P$ (0.1 M). The solutions were sparged with N_2 for 15 min prior to irradiation, where the headspace was filled with N_2. Oxygen free conditions were needed otherwise the sensitizer **1** produces singlet oxygen under aerobic conditions.[15] Phosphorous trapping agents such as trimethyl phosphite have been reported to trap the alkoxy radicals,[35] and thus were used here. The product $(MeO)_3P{=}O$ was monitored by GC/MS and ^1H and ^{31}P NMR spectroscopy. The peroxide decomposition yields did not vary by more than 1% between the two methods: GC/MS and ^1H NMR spectroscopy. The use of ^{31}P NMR spectroscopy produced higher error (~2-3%). GC/MS and ^1H NMR spectroscopy were also used to characterize the hydrocarbon products.

Heterogeneous Method. The preparation of 4,4′-dimethylbenzil **1** and dicumyl peroxide **3** co-adsorbed onto fumed silica has been described previously.[17] Briefly, fumed silica was immersed in a dichloromethane solution of solvated **1** and **3**. After stirring, the dichloromethane was evaporated with a stream of N_2 gas leaving reagents adsorbed on the silica. The silica particles were further dried under vacuum. Compound adsorption was assumed to be uniform. We used a 20-cm^3 glass container containing 100-mg silica particles adsorbed with **1** and **3** that form a two-phase system that was N_2-degassed. This container was rotated by its attachment to a stirring paddle where the silica particles tumbled during the irradiation for 1 h. Once the photolysis was completed after 1 h, products **6**–**8** were detected upon desorption from the silica surface with dichloromethane or methanol and filtered with a syringe-loaded filter. Here, we monitored the

consumption of dicumyl peroxide **3** over time and quantitated the products formed based on GC/MS and NMR. The possible formation of volatile products was not explored.

ORCID

Alexander Greer: 0000-0003-4444-9099

Acknowledgements

We thank the National Science Foundation (CHE-1856765) and PSC-CUNY for funding. We also thank Leda Lee for the graphic arts work and a reviewer for their comments.

Supporting Information

Additional supporting information may be found online in the Supporting Information section at the end of the article:

Figure S1. Schematic of the photoreactor setup.

Figure S2. ^{1}H NMR spectra of $(MeO)_3P$ and phosphorane **4** in CD_3CN.

Figure S3. ^{1}H NMR spectra of 4,4'-dimethylbenzil **1** and phosphorane **4** in CD_3CN.

Figure S4. ^{31}P NMR spectra of $(MeO)_3P$, $(MeO)_3P{=}O$, and phosphorane **4** in CD_3CN.

Figure S5. Absorption spectra of reagents, products, and filter solution in CH_3CN.

Figure S6. Absorption and fluorescence spectra of 4,4'-dimethylbenzil **1** in CH_3CN.

Figure S7. Absorption spectra of the reaction mixture of 1 with $(MeO)_3P$ in CH_3CN.

Figure S8. Kinetic plot and R square fitting of the kinetic data.

References

(1) Celli, J. P.; Spring, B. Q.; Rizvi, I.; Evans, C. L.; Samkoe, K. S.; Verma, S.; Pogue, B. W.; Hasan, T. Imaging and Photodynamic Therapy: Mechanisms, Monitoring, and Optimization. *Chem. Rev.* **2010**, *110*, 2795-2838, DOI: 10.1021/cr900300p

(2) Rai, P.; Mallidi, S.; Zheng, X.; Rahmanzadeh, R.; Mir, Y.; Elrington, S.; Khurshid, A.; Hasan, T. Development and Applications of Photo-triggered Theranostic Agents. *Adv. Drug Deliv. Rev.* **2010**, *62*, 1094-1124, DOI: 10.1016/j.addr.2010.09.002

(3) Amirshaghaghi, A.; Yan, L.; Miller, J.; Daniel, Y.; Stein, J. M.; Busch, T. M.; Cheng, Z.; Tsourkas, A. Chlorin e_6-Coated Superparamagnetic Iron Oxide Nanoparticle (SPION) Nanoclusters as a Theranostic Agent for Dual-Mode Imaging and Photodynamic Therapy. *Sci. Rep.* **2019**, *9*, 1-9, DOI: 10.1038/s41598-019-39036-1

(4) Sainuddin, T., M. Pinto, H. Yin, M. Hetu, J. Colpitts and S. A. McFarland Strained Ruthenium Metal–Organic Dyads as Photocisplatin Agents with Dual Action. *J. Inorg. Biochem.* **2016**, *158*, 45-54, DOI: 10.1016/j.jinorgbio.2016.01.009

(5) Albani, B. A.; Pena, B.; Leed, N. A.; de Paula, N. A. B. G.; Pavani, C.; Baptista, M. S.; Dunbar, K. R.; Turro, C. Marked Improvement in Photoinduced Cell Death by a New Tris-heteroleptic Complex with Dual Action: Singlet Oxygen Sensitization and Ligand Dissociation. *J. Am. Chem. Soc.* **2014**, *136*, 17095-17101, DOI: 10.1021/ja508272h

(6) Brega, V.; Scaletti, F.; Zhang, X.; Wang, L.; Li, P.; Xu, Q.; Rotello, V. M.; Thomas, S. W. Polymer Amphiphiles for Photoregulated Anticancer Drug Delivery. *ACS Appl. Mater. Interfaces* **2019**, *11*, 2814-2820, DOI: 10.1021/acsami.8b18099

(7) Hirsch, D. R.; Schiavone, D. V.; Berkowitz, A. J.; Morrison, L. A.; Masaoka, T.; Wilson, J. A.; Lomonosova, E.; Zhao, H.; Patel, B. S.; Dalta, S. H.; Majidi, S. J.; Pal, R.; K.; Gallicchio, E.; Tang, L.; Tavis, J. E.; Le Grice, S. F. J.; Beutler, J. A.; Murelli, R. P. Synthesis and Biological Assessment of 3,7-Dihydroxytropolones. *Org. Biomol. Chem.* **2018**, *16*, 62-69, DOI: 10.1039/C7OB02453C

(8) Mousset, C.; Giraud, A.; Provot, O.; Hamze, A.; Bignon, J.; Liu, J.; Thoret, S.; Dubois, J.; Brion, J.; Alami, M. Synthesis and Antitumor Activity of Benzils Related to Combretastatin A-4. *Bioorg. Med. Chem. Lett.* **2008**, *18*, 3266-3271, DOI: 10.1016/j.bmcl.2008.04.053

(9) Bhanthumnavin, W.; Bentrude, W. G. Photo-Arbuzov Rearrangements of 1-Arylethyl Phosphites: Stereochemical Studies and the Question of Radical-Pair Intermediates. *J. Org. Chem.* **2001**, *66*, 980-990, DOI: 10.1021/jo001545e

(10) Hager, D. C.; Bentrude, W. G. Triplet-Sensitized Photorearrangements of Six-Membered-Ring 2-Phenylallyl Phosphites. Reaction Efficiency and Stereochemistry at Phosphorus. *J. Org. Chem.* **2000**, *65*, 2786-2791, DOI: 10.1021/jo9918302

(11) Osman, F. H.; El-Samahy, F. A. The Behavior of 3,3-Diphenylindan-1,2-dione Towards Alkyl Phosphites. *Monatsh. Chem.* **2007**, *138*, 973-978, DOI: 10.1007/s00706-007-0692-4

(12) Mahran, M. R.; Abdou, W. M.; Khidre, M. D. Organophosphorus Chemistry. XII. Reaction of Furil with Alkyl Phosphites and Ylide-Phosphoranes. *Monatsh. Chem.* **1990**, *121*, 51-58, DOI: 10.1007/BF00810294

(13) Ramasamy, E.; Jayaraj, N.; Porel, M.; Ramamurthy, V. Excited State Chemistry of Capsular Assemblies in Aqueous Solution and on Silica Surfaces. *Langmuir* **2012**, *28*, 10-16, DOI: 10.1021/la203419y

(14) Ramamurthy, V. Photochemistry within a Water-Soluble Organic Capsule. *Acc. Chem. Res.* **2015**, *48*, 2904-2917, DOI: 10.1021/acs.accounts.5b00360

(15) Natarajan, A.; Kaanumalle, L. S.; Jockusch, S.; Gibb, C. L. D.; Gibb, B.C.; Turro, N. J.; Ramamurthy, V. Controlling Photoreactions with Restricted Spaces and Weak Intermolecular Forces: Exquisite Selectivity during Oxidation of Olefins by Singlet Oxygen. *J. Am. Chem. Soc.* **2007**, *129*, 4132-4133, DOI: 10.1021/ja070086x

(16) Malval, J.; Dietlin, C.; Allonas, X.; Fouassier, J. Sterically Tuned Photoreactivity of an Aromatic α-diketone Family. *J. Photochem. Photobiol. A* **2007**, *192*, 66-73, DOI: 10.1016/j.jphotochem.2007.05.005

(17) Walalawela, N.; Greer, A. Heterogeneous Photocatayltic Deperoxidation with UV and Visible Light. *J. Phys. Org. Chem.* **2018**, e3807, DOI: 10.1002/poc.3807

(18) Ding, B.; Bentrude, W. G. Trimethyl Phosphite as a Trap for Alkoxy Radicals Formed from the Ring Opening of Oxiranylcarbinyl Radicals. Conversion to Alkenes. Mechanistic Applications to the Study of C–C versus C–O Ring Cleavage. *J. Am. Chem. Soc.* **2003**, *125*, 3248-3259, DOI: 10.1021/ja020761x

(19) Fasciani, C.; Alejo, C. J. B.; Grenier, M.; Netto-Ferreira J. C.; Scaiano, J. C. High-Temperature Organic Reactions at Room Temperature using Plasmon Excitation: Decomposition of Dicumyl Peroxide. *Org. Lett.* **2010**, *13*, 204-207, DOI: 10.1021/ol1026427

(20) Lazár, M.; Matisová-Rychlá, L.; Ďurdovič, V.; Rychlý, J. Chemiluminescence in the Thermal Decomposition of Dicumyl Peroxide. *J. Lumin.* **1974**, *9*, 240-248, DOI: 10.1016/0022-2313(74)90052-0

(21) Abd-Alla, M. A. Novel Synthesis of Poly(benzoin) and Poly(benzil). Characterization and Application as Photosensitizer Materials. *Macromol. Chem. Phys.* **1991**, *192*, 277-283, DOI: 10.1002/macp.1991.021920209

(22) Rowe, P. D.; Thomas, D. K. The Thermal Decomposition of Dicumyl Peroxide in Polyethylene Glycol and Polypropylene Glycol. *J. Appl. Polym. Sci.* **1963**, *7*, 461-468, DOI: 10.1002/app.1963.070070205

(23) Callaghan, S.; Senge, M. O. The Good, the Bad, and the Ugly – Controlling Singlet Oxygen Through Design of Photosensitizers and Delivery Systems for Photodynamic Therapy. *Photochem. Photobiol. Sci.* **2018**, *17*, 1490-1514, DOI: 10.1039/C8PP00008E

(24) Röder, B.; Büchner, M.; Rückmann, I.; Senge, M. O. Correlation of Photophysical Parameters with Macrocycle Distortion in Porphyrins with Graded Degree of Saddle Distortion. *Photochem. Photobiol. Sci.* **2010**, *9*, 1152-1158, DOI: 10.1039/C0PP00107D

(25) Kielmann, M.; Grover, N.; Kalish, W. W.; Senge, M. O. Incremental Introduction of Organocatalytic Activity into Conformationally Engineered Porphyrins. *Eur. J. Org. Chem.* **2019**, 2448-2452, DOI: 10.1002/ejoc.201801691

(26) Pistner, A. J.; Pupillo, R. C.; Yap, G. P. A.; Lutterman, D. A.; Ma, Y.; Rosenthal, J. Electrochemical, Spectroscopic, and $^1O_2$ Sensitization Characteristics of 10,10-Dimethylbiladiene Complexes of Zinc and Copper. *J. Phys. Chem. A* **2014**, *118*, 10639-10648, DOI: 10.1021/jp506412r

(27) Manini, P.; Bietti, M.; Galeotti, M.; Salamone, M.; Lanzalunga, O.; Cecchini, M.M.; Reale, S.; Crescenzi, O.; Napolitano, A.; De Angelis, F.; Barone, V.; D'Ischia, M. Characterization and Fate of Hydrogen-Bonded Free-Radical Intermediates and Their Coupling Products from

the Hydrogen Atom Transfer Agent 1,8-Naphthalenediol. *ACS Omega* **2018**, *3*, 3918-3927, DOI: 10.1021/acsomega.8b00155

(28) Shah, B. K.; Gusev, A.; Rodgers, M. A. J.; Neckers, D. C. Ultrafast Pump-Probe Studies of tert-Butyl Aroylperbenzoates and Triplet Energy Interception by the O–O Bond. *J. Phys. Chem. A* **2004**, 108, 5926-5931, DOI: 10.1021/jp049588c

(29) Scaiano, J. C.; Connolly, T. J.; Mohtat, N.; Pliva, C. N. Exploratory Study of the Quenching of Photosensitizers by Initiators of Free Radical "Living" Polymerization. *Can. J. Chem.* **1997**, *75*, 92-97.

(30) Morlet-Savary, F.; Wieder, F.; Fouassier, J. P. Sensitized Dissociation of Peroxides and Peresters in the Presence of Thiopyrylium Salts. *J. Chem. Soc. Faraday Trans.* **1997**, *93*, 3931-3937, DOI: 10.1039/A704951J

(31) Nau, W. M.; Scaiano, J. C. Oxygen Quenching of Excited Aliphatic Ketones and Diketones. *J. Phys. Chem.* **1996**, *100*, 11360-11367, DOI: 10.1021/jp960932i

(32) Engel, P. S.; Woods, T. L.; Page, M. A. Quenching of Excited Triplet Sensitizers by Organic Peroxides. *J. Phys. Chem.* **1983**, *87*, 10-13, DOI: 10.1021/j100224a004

(33) Walling, C.; Gibian, M. J. The Photosensitized Decomposition of Peroxides. *J. Am. Chem. Soc.* **1965**, *87,* 3413-3417, DOI: 10.1021/ja01093a022

(34) Mohapatra, P. P.; Chiemezie, C. O.; Kligman, A.; Kim, M. M.; Busch, T. M.; Zhu, T. C.; Greer, A. ^{31}P NMR Evidence for Peroxide Intermediates in Lipid Emulsion Photooxidations: Phosphine Substituent Effects in Trapping. *Photochem. Photobiol.* **2017**, *93*, 1430-1438, DOI: 10.1111/php.12810

(35) Jiao, X.; Bentrude, W. G. A Facile Route to Vinyl- and Arylphosphonates by Vinyl and Aryl Radical Trapping with $(MeO)_3P$. *J. Org. Chem.* **2003**, *68*, 3303-3306, DOI: 10.1021/jo020671a

(36) Gaussian 09, Revision D.01, Frisch, M. J.; Trucks, G. W.; Schlegel, H. B.; Scuseria, G. E.; Robb, M. A.; Cheeseman, J. R.; Scalmani, G.; Barone, V.; Mennucci, B.; Petersson, G. A.; Nakatsuji, H.; Caricato, M.; Li, X.; Hratchian, H. P.; Izmaylov, A. F.; Bloino, J.; Zheng, G.; Sonnenberg, J. L.; Hada, M.; Ehara, M.; Toyota, K.; Fukuda, R.; Hasegawa, J.; Ishida, M.; Nakajima, T.; Honda, Y.; Kitao, O.; Nakai, H.; Vreven, T.; Montgomery, J. A., Jr.; Peralta, J. E.; Ogliaro, F.; Bearpark, M.; Heyd, J. J.; Brothers, E.; Kudin, K. N.; Staroverov, V. N.; Kobayashi, R.; Normand, J.; Raghavachari, K.; Rendell, A.; Burant, J. C.; Iyengar, S. S.; Tomasi, J.; Cossi, M.; Rega, N.; Millam, M. J.; Klene, M.; Knox, J. E.; Cross, J. B.; Bakken, V.; Adamo, C.; Jaramillo, J.; Gomperts, R.; Stratmann, R. E.; Yazyev, O.; Austin, A. J.; Cammi, R.; Pomelli, C.; Ochterski, J. W.; Martin, R. L.; Morokuma, K.; Zakrzewski, V. G.; Voth, G. A.; Salvador, P.; Dannenberg, J. J.; Dapprich, S.; Daniels, A. D.; Farkas, Ö.; Foresman, J. B.; Ortiz, J. V.; Cioslowski, J.; Fox, D. J. Gaussian, Inc., Wallingford CT, 2009

(37) Dennington, R.; Keith, T.; Millam, J. Gaussview. Semichem Inc., Shawnee Mission KS, 2009.

Table of Contents Graphic